Fluctuation correlation spectroscopy for the advanced physics laboratory

Robert Rieger and Carlheinz Röcker
Department of Biophysics, University of Ulm, 89069 Ulm, Germany

G. Ulrich Nienhaus
Department of Biophysics, University of Ulm, 89069 Ulm, Germany
and Department of Physics, University of Illinois at Urbana-Champaign, Urbana, Illinois 61801

(Received 16 May 2005; accepted 19 August 2005)

A fluorescence correlation spectrometer is developed that is suitable for use in advanced laboratory courses. The instrument is simple to build and understand and can be constructed at a small fraction of the cost of a commercial or research-grade instrument. We demonstrate its surprisingly high performance with a simple biophysics application, the study of the binding of two complementary DNA strands. The instrument will be useful in areas of physics where precise measurements of the dynamics of fluorescent (or fluorescently labeled) molecules or nanoparticles in solution are of interest. © *2005 American Association of Physics Teachers.*
[DOI: 10.1119/1.2074047]

I. INTRODUCTION

Although Einstein's legendary papers on quantum theory and special relativity have fascinated scientists and laypersons alike, his explanation of Brownian motion[1] also heralded a revolution in physical thought. From our one hundred year perspective, it seems remarkable that the atomic hypothesis was still hotly debated at the turn of the twentieth century. Einstein's theory together with its subsequent experimental verification by Jean Perrin[2] finally led to the universal acceptance of the existence of atoms and molecules.

By using a statistical mechanics description, Einstein showed that the irregular motion of particles suspended in solution can be explained as arising from the random thermal action of the solvent molecules on these particles, so that the solvent molecules act both as the driving force for the Brownian fluctuations and as a means of damping the motion. From these considerations, Einstein derived the Stokes-Einstein relation as the first example of a fluctuation-dissipation theorem,

$$D = \frac{k_B T}{6\pi\eta R}, \tag{1}$$

where D is the translational diffusion coefficient, R is the radius of the suspended particle, k_B is Boltzmann's constant, T is the absolute temperature, and η the solvent viscosity. He then showed that the mean-squared displacement increases linearly in time and is proportional to D,

$$\langle x^2 \rangle = 2Dt \quad \text{(one dimension)}. \tag{2}$$

The success of Einstein's mechanics to explain Brownian motion also removed all doubts concerning the validity of Boltzmann's statistical interpretation of the laws of thermodynamics.

Our aim is to develop an experiment for the advanced physics laboratory by which these fundamental aspects can be studied. Fluorescence correlation spectroscopy is an attractive and sophisticated approach for addressing these issues and is based on optical detection at the level of single molecules. The equipment is typically very expensive so that it is normally available only in research laboratories. However, we have developed a compact fluorescence correlation spectroscopy apparatus with real time processing and display of the correlation function that is surprisingly affordable and yet provides excellent performance. With this apparatus, students can acquire familiarity with modern optics, which is of much relevance in many areas of science and industry. Moreover, exposure to correlation analysis to extract information on molecular dynamics from random fluctuations is relevant to other areas of physics.

In this paper we sketch the theoretical background of fluorescence correlation spectroscopy, describe the construction of the instrument and software, and give some basic applications. A simple experiment measuring the diffusion of Rhodamine 6G (R6G) demonstrates the excellent performance of the apparatus and is useful for calibration of the instrument. A second example from biophysics gives a starting point for the development of further applications.

II. FLUCTUATION CORRELATION SPECTROSCOPY

Fluctuation correlation spectroscopy is based on the measurement of equilibrium fluctuations.[3] The technique was introduced more than 30 years ago,[4] but became popular only recently, after it was implemented in a confocal microscope geometry, yielding volumes in the 1 μm^3 range from which fluorescence light is collected.[5] The design and technical improvements of detectors, correlators, and microscope objectives in recent years has established fluctuation correlation spectroscopy as a powerful method for the determination of dynamic properties of particles in solution, featuring single-molecule sensitivity and impressively short acquisition times of only a few seconds.

In a typical fluctuation correlation spectroscopy experiment, fluorescence photons emanating from a femtoliter-sized open volume within the sample solution are counted as a function of time. The observation volume is created by tight focusing of laser light into the solution in conjunction with detection through a confocal pinhole. The technique is based on the analysis of the fluctuations of the fluorescence intensity emitted by individual molecules or small ensembles in thermodynamic equilibrium. These fluctuations may be caused by fluorescent molecules entering and leaving the open observation volume due to Brownian motion. Physical or chemical transitions of molecules to a state with altered fluorescence properties during their transit through the obser-

 © 2005 American Association of Physics Teachers

vation volume will also cause fluorescence fluctuations. We can determine diffusion coefficients as well as rate coefficients of photophysical or chemical reactions by correlation analysis of the equilibrium fluctuations. In this paper, we focus on Brownian motion as the only source of fluorescence fluctuations.

The normalized autocorrelation function, $G(\tau)$, of the fluorescence fluctuations is calculated from the fluorescence intensity, $F(t)$, as

$$G(\tau) = \frac{\langle \delta F(t)\, \delta F(t+\tau) \rangle}{\langle F(t) \rangle^2}. \tag{3}$$

The fluctuations $\delta F(t) = F(t) - \langle F(t) \rangle$ are the deviations of the measured fluorescence intensity from its time average. The temporal decay of $G(\tau)$ contains information about the characteristic time scales of the dynamic processes causing the fluorescence fluctuations.

The fluorescence intensity fluctuations can be calculated by spatial integration of the concentration fluctuations, $\delta c(\mathbf{r},t)$, weighted by the sensitivity function, $\Phi(\mathbf{r})$, of the volume, which gives the probability of detecting a photon from a particular volume element,

$$\delta F(t) = \int\int\int \Phi(\mathbf{r})\, \delta c(\mathbf{r},t)\, d\mathbf{r}. \tag{4}$$

The size of the observation volume is thus defined by $\Phi(\mathbf{r})$, which for simplicity is usually approximated by a three-dimensional Gaussian, with the parameters r_0, z_0 representing the radial and axial distances over which the intensity decays by a factor of $1/e^2$. The radial distance r_0 is governed by the size of the focused laser spot and thus the numerical aperture of the objective lens; the axial distance is determined by the size of the confocal detection pinhole (*vide infra*). The concentration fluctuations are governed by Fick's law,

$$\frac{\partial \delta c(\mathbf{r},t)}{\partial t} = D \nabla^2 \delta c(\mathbf{r},t). \tag{5}$$

From Eqs. (3)–(5), the autocorrelation function for translational diffusion can be calculated as[5,6]

$$G(\tau) = \frac{1}{N}\left[1 + \frac{\tau}{\tau_D}\right]^{-1}\left[1 + \frac{\tau}{\tau_D}\left(\frac{r_0}{z_0}\right)^2\right]^{-1/2}. \tag{6}$$

Here, $N = cV_{\text{eff}}$ is the mean number of particles in the effective observation volume, $V_{\text{eff}} = \pi^{3/2} r_0^2 z_0^2$. The correlation time for translational diffusion, τ_D, is given by [compare to Eq. (2)],

$$\tau_D = \frac{r_0^2}{4D}. \tag{7}$$

A nonlinear least-squares fit of the model function, Eq. (6), to the experimental autocorrelation curve yields the free parameters, N, τ_D, and the aspect ratio $\omega = r_0/z_0$. Usually, we determine the geometrical parameters r_0 and ω of the fluorescence correlation spectroscopy apparatus by a calibration experiment with particles of known diffusion coefficient, D. Subsequently, $G(\tau)$ is measured for the particles of interest and only τ_D is varied in the fit; D is then calculated from Eq. (7). The radius R of the particle is subsequently obtained from the Stokes-Einstein relation, Eq. (1). We usually refer more precisely to R_H, the radius of the hydrated (or more generally, solvated) particle to account for the fact that the particle drags its solvent layer along its trajectory and thus appears somewhat larger. In addition to the temporal decay of $G(\tau)$, the fluctuation amplitude can be analyzed. This quantity is represented by the autocorrelation amplitude at early times, $G(0)$, which is inversely related to the average number of molecules, N, in the observation volume (typically 0.1–10 molecules).

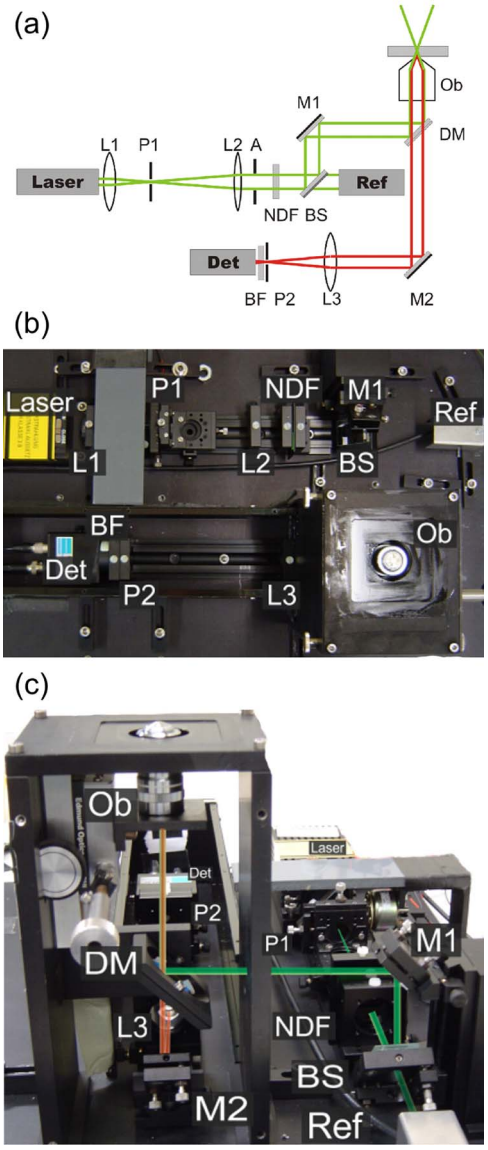

Fig. 1. (a) Schematic drawing of the optical setup of the fluorescence correlation spectrometer. (b) Photograph of the fluorescence correlation spectroscopy setup as viewed from the top. (c) Side view of the instrument, with the cover removed from the tower for better view. The beams have been added to illustrate the optical pathways.

III. DESCRIPTION OF THE APPARATUS

A. Optical setup

We have developed a simple, low-cost fluorescence correlation spectroscopy apparatus utilizing our experience gained in spectroscopy research.[7–11] The optical design is shown schematically in Fig. 1(a) and the essential components are listed in Table I. Figures 1(b) and 1(c) show photographs of

Table I. Essential components for the fluorescence correlation spectroscopy apparatus.

Component (Model)	Manufacturer/Vendor	Est. price ($)
20 mW DPSS 532 nm Laser	Laserlight Showdesign, Berlin, Germany also Laser Light Shows, Toronto, Canada	680
Objective, DIN 100×/1.25 oil (J36-134)	Edmund Scientific	300
Immersion Oil, Immersol 518F	Carl Zeiss, Thornwood, NY	30
Objective mover (J37-603)	Edmund Scientific	190
Photon counting head (H7155)	Hamamatsu	1850
Si photodiode (FDS1010)	Thorlabs	200
32 bit counter/timer card (PCI-6602)	National Instruments	710
Dichroic mirror (DT-Red, 38 4082 033)	Linos Photonics	20
Bandpass filter (HQ 545 LP)	Chroma	270
Optical mounts, lenses, pinholes	Owis, Linos Photonics, Thorlabs	1500

the arrangement of the optical components in top view and side view, respectively. The beam from a small diode-pumped, solid-state (DPSS) Nd-YAG laser (532 nm, 20 mW) is spatially filtered and expanded by lens L1 (f_1 = 60 mm), pinhole P1 (20 μm diam), and lens L2 (f_2 = 100 mm), and then passed through aperture A. These optical elements provide a pure TEM00 spatial beam mode. The beam diameter is chosen to fill the back aperture plane of the objective to achieve a minimal spot size in the sample. By means of a neutral density filter, the laser power is decreased by ~2 orders of magnitude so that the sample is irradiated with ~100 μW of light during data acquisition. After passing a 70/30 beam splitter (BS)-mirror (M1) combination acting as a beam elevator, the excitation light is reflected by a dichroic mirror (DM) into the high numerical aperture (NA = 1.25) oil immersion objective (Ob). Note that low-fluorescence immersion oil is required to achieve high sensitivity (Table I). The red-shifted fluorescence emanating from the sample is collected by the same objective, transmitted through the dichroic mirror (DM), reflected by mirror M2 and focused by lens L3 (f_3 = 150 mm) onto the confocal pinhole P2 (50 μm diameter). A blocking filter (BF) removes the scattered laser light at 532 nm; finally, the fluorescence photons are detected by a photomultiplier tube (PMT) integrated into a photon counting head (Det). The light that passes the beam splitter (BS) is registered with a photodiode to monitor fluctuations in the laser intensity.

As seen in Figs. 1(b) and 1(c), the setup consists of two parallel mounting rails for the excitation and the detection path and a 20 cm high tower [bottom right of Fig. 1(b)], carrying the parts shared by excitation and detection, that is, the dichroic mirror, the objective lens, and the sample on top of the tower. All optical components are mounted on an aluminum base plate of 40×60 cm^2.

B. Alignment procedure

After alignment of the spatial filter, the excitation beam path is aligned by adjusting the beam splitter and mirror M1 to steer the beam into the back aperture plane of the objective along the optical axis. The glass-air interface of a cover slip is used as a reflective sample for this purpose. The reflected light is observed below the dichroic mirror while moving the objective lens up and down. Good alignment yields a symmetric fringe pattern without shifting of the central spot when the focus is passed. Because only the weak transmission of laser light through the dichroic mirror is used to align the optics, the neutral density filter (NDF) is removed for this step.

To align the detection path, the detector and blocking filter are removed so that the light passing through confocal pinhole P2 can be imaged on a piece of white paper. The mirror M2 is tuned until the light from the pinhole shows a bright spot and a symmetric diffraction pattern when the objective is moved up and down. After reinstalling the blocking and neutral density filters and the detector, the instrument is screened from ambient light and then is ready for use.

IV. REALTIME PROCESSING USING A SOFTWARE CORRELATOR

TTL signals from the photon counting head are fed into a standard counter/timer card (NI PCI-6602), where they are further processed by a software correlator written using LABVIEW and an algorithm that simulates the function of a hardware correlator.[12] For each time interval k, the number of events within this interval, n_i, is collected and referred to as a data point in the following. The most recent data point is multiplied by its 20 predecessors, which are stored in a shift register. This data point is then stored in the first position of the shift register after moving all other points one position back and discarding the oldest point. This procedure is repeated M times, and the products are summed over time, yielding the raw autocorrelation function,

$$G^{\mathrm{raw}}(k) = \sum_{i=1}^{M} n_i n_{i-k}. \tag{8}$$

We convert G^{raw} to $G(k)$ using the relation

$$G(k) = \frac{M G^{\mathrm{raw}}(k)}{M_0 M_k} - 1, \tag{9}$$

with $M_0 = \Sigma_{i=1}^{M} n_i$ and $M_k = \Sigma_{i=1}^{M} n_{i-k}$. To increase the dynamic range, we use five independent sub-correlators with different sampling times, spanning five orders of magnitude in correlation time. This algorithm is surprisingly effective though certainly not the most elegant. With a 1 GHz personal computer and 512 Mb of RAM, we were able to reliably record data with a minimal lag time, τ_{min}, of ~3 μs. For shorter measurements, up to a total duration of ~10 s, τ_{min} was ~2 μs. The time resolution of the instrument is limited to ~1 μs due to after-pulsing of the photomultiplier, and there-

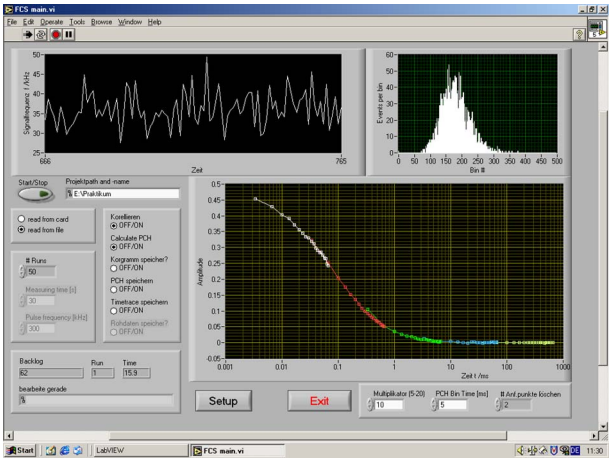

Fig. 2. User interface of the software correlator displaying a measurement on an aqueous solution of Rhodamine 6G. The time trace of the detector signal is shown in the upper left panel. On the right, the photon counting histogram (PCH) is displayed. The main part of the screen is taken up by the display of the intensity autocorrelation function.

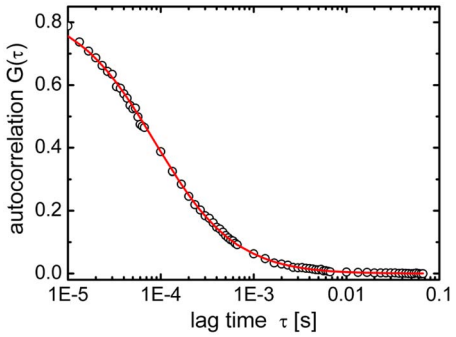

Fig. 3. Autocorrelation function for Brownian motion of Rhodamine 6G in water. The model function for translational diffusion perfectly describes the experimental result.

fore, the restrictions due to the software correlation are minimal and can be completely removed by using a faster computer. For even faster time scales, we could change the algorithm from photon counting mode to time measuring mode, as described in Ref. 13.

The user interface is shown in Fig. 2. The largest subpanel is for the display of the autocorrelation function in real time during the measurements. It shows how the autocorrelation function emerges out of the noise within seconds. In addition, the measured photon flux is continuously displayed as a function of time in the upper left. The fluorescence emission time trace is conveniently used for alignment purposes. For example, the axial objective position that provides the smallest possible observation volume is simply found by adjusting the objective for maximum intensity. Note that the autocorrelation function cannot be used for this purpose, because it represents intensity fluctuations and not the intensity itself, and it does not reflect the immediate situation but rather comprises all the data since the start of the measurement. Inspection of the time trace is also helpful for detecting the formation of aggregates in the sample, as they give rise to intense spikes. Large, bright particles cause pronounced distortions of the autocorrelation function and should be removed by filtering the sample solutions. A photon counting histogram is generated in the upper right of the display panel. It shows the probability of detecting a certain number of photons within a given time interval and is a measure of the relative brightness of the detected molecules.[14,15]

If the sample contains only one kind of fluorescing particles, the histogram is close to a Poisson distribution. A mixture of species (differing in fluorescence efficiency) yields additional peaks in the histogram or a broadening of the distribution. The photon counting histogram is thus an alternative to autocorrelation analysis and can be used to separate particles on the basis of their brightness instead of their size.[9,10]

The user interface lets us see the interrelations between the photon time trace, the correlation function, and the photon counting statistics. If, for example, a bright aggregate of particles passes through the detection volume, a large spike is observed in the time trace, an additional slow component appears in the correlation window, and data at high counting rates appear in the photon counting histogram. These three functions can be stored in a data file for further analysis.

V. FLUORESCENCE CORRELATION SPECTROSCOPY EXPERIMENTS

A. Sample preparation

We discuss two simple fluorescence correlation spectroscopy experiments to demonstrate the quality of the apparatus. For those not familiar with the preparation of sample solutions containing biomolecules, we suggest consulting textbooks for some basic procedures.[16] The sample solutions are prepared in a sandwich cell, which consist of two microscope cover slips, separated by two stripes of double-sided adhesive tape ($\sim$200 μm thick), leaving a $\sim$2 mm wide sample channel in between. Prior to the measurements, the cell is filled with a 1 mg/ml solution of bovine serum albumin (BSA) protein[17] for 5 min. BSA adsorbs to the glass surface, which prevents further adsorption of the sample material. This procedure is important in practice because of the large surface-to-volume ratio and the small (nanomolar) sample concentrations. After thorough washing with a buffer, the cell is filled with the sample, mounted on top of the objective and is ready for measurements.

B. Brownian motion of fluorescent dye molecules

Rhodamine 6G (R6G) is a fluorescent organic dye that is suitable for excitation at 532 nm. It emits bright fluorescence around 560 nm in aqueous solution. Its diffusion coefficient is 2.8×10^{-10} m^2 s^{-1} in water at 22 °C,[5] and we use R6G to characterize the observation volume. Figure 3 shows a typical autocorrelation function for the Brownian motion of R6G, collected in $\sim$100 s. It can be well described by the model function for translational diffusion, Eq. (6), with fit parameters τ_D=85.0 μs and ω=0.11. From these data, we obtain r_0=0.30 μm and z_0=2.8 μm, and an effective volume V_{eff}=1.4 fl. From the amplitude, $G(0)$, we obtain an average number of molecules, N=1.2, in the detection volume, corresponding to an average concentration of 1.4 nM. This experiment exemplifies the rule of thumb that a particle concentration of 1 nM in the solution yields an average occupancy of one particle in the observation volume.

Following this calibration measurement, unknown samples can be measured in the well-defined observation geometry. The geometrical parameters are held fixed in the

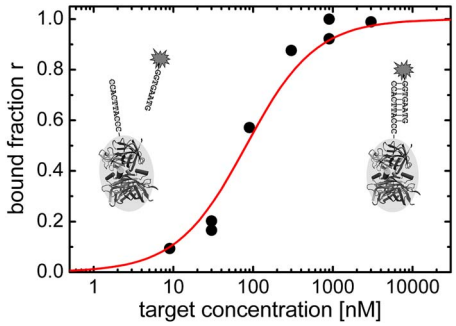

Fig. 4. Saturation curve for the binding of an octameric, fluorescently labeled DNA strand to its complementary strand. In the insets, the molecular species are depicted for the free (left) and the bound (right) state. The substantial increase in the mass of the fluorescent entity markedly slows the Brownian motion of the bound species.

analysis, and the measured correlation times are converted into diffusion coefficients using Eq. (7). We note that changes in the objective position with respect to the sample should be minimized because the observation volume changes with the depth of the focus in the sample solution.

C. Intermolecular interaction – DNA duplex formation

The second experiment shows how molecular interactions can be studied via their effects on Brownian diffusion. Complementary deoxyribonucleic acid (DNA) oligomers, which can be ordered from many biotech companies, will form duplexes in solution, and their mutual binding affinity can be determined from the decrease in mobility upon binding of a fluorescently labeled DNA-strand to its unlabeled complementary strand. As a fluorescent DNA-strand, we chose an octameric oligonucleotide, labeled with a fluorophore (Alexa Fluor 555) at the 5' end (DNA-F, 5'-Alexa555-GGTGAATG).[18] For the complementary strand, an octamer was obtained that had a biotin molecule attached at the 5' end (DNA-B, 5'-Biotin-TEG-CCCATTCACC).[18] The protein streptavidin binds to biotin very strongly,[19] and thus the mass of this particle can be substantially increased by adding streptavidin to the solution, which was done at twice the concentration of the octamer. Depictions of the molecules are shown as insets in Fig. 4. For the experiments, we used a buffer solution containing 2 M KCl, 12 mM $MgCl_2$, and 5 mM Tris, adjusted to pH 7.4.

For this fluorescence correlation spectroscopy measurement on the fluorescently labeled DNA-octamer in the presence of the unlabeled complementary DNA, we expect that the autocorrelation function can be expressed as a superposition of two terms, each component being described by $G(\tau)$ as given in Eq. (6), with correlation times, τ_1, for the single-stranded DNA-F and τ_2 for the double stranded DNA,

$$G(\tau)=\frac{1}{N}\left[(1-f)\left(1+\frac{\tau}{\tau_1}\right)^{-1}\left(1+\frac{\tau}{\tau_1}\omega^2\right)^{-1/2}+f\left(1+\frac{\tau}{\tau_2}\right)^{-1}\left(1+\frac{\tau}{\tau_2}\omega^2\right)^{-1/2}\right]. \tag{10}$$

We note that the correlation times τ_1 and τ_2, (180±10) μs and (510±20) μs in this experiment, respectively, can be determined from separate measurements of the pure single- and double-stranded species. The latter species is obtained at a high concentration of the complementary strand, whereas the aspect ratio ω is measured in the calibration experiment with R6G. Therefore, only the bound fraction, f, of fluorescently labeled DNA and the number of fluorescent molecules N are free parameters in the two species-autocorrelation function, Eq. (10).

To characterize the binding affinity for the duplex formation, a series of measurements was performed, keeping the concentration of fluorescently labeled DNA constant at 3 nM, and varying the concentration of the complementary or target strand over a wide range of concentrations. The data in Fig. 4 show that the bound fraction, f, increases with the concentration of the target strand (DNA-B). This behavior can be described by a simple bimolecular binding model that derives from the law of mass action,

$$f=\frac{[\text{DUPLEX}]}{[\text{DUPLEX}]+[\text{DNA-F}]}=\frac{1}{1+K_D/[\text{DNA-B}]}, \tag{11}$$

with the binding affinity characterized by the equilibrium dissociation coefficient,

$$K_D=\frac{[\text{DNA-F}]\cdot[\text{DNA-B}]}{[\text{DUPLEX}]}. \tag{12}$$

Equation (11) shows that K_D represents the concentration of free DNA-B, at which half of the DNA-F molecules are bound in the double stranded DNA. The solid line in Fig. 4 is a fit to this relation, yielding K_D=(82±13) nM.

VI. CONCLUSIONS

We have described the development of a reliable fluorescence correlation spectroscopy apparatus with excellent performance at a very moderate price. This apparatus may be attractive for physics educators who have only a limited budget for instrumentation. In the Appendix we provide additional information on the components. The design can easily be modified. For example, the PMT module can be replaced by a much more expensive silicon avalanche photodiode module or can be built from less expensive parts by someone with some experience in electronics.

Fluorescence correlation spectroscopy is a powerful method for studying a wide range of phenomena. We have discussed two simple applications, the measurement of diffusion of a dye molecule in water, and the binding of two short, complementary DNA oligonucleotides. Many other applications can be found in the literature,[3,7–11] and more experiments with other biological or nonbiological nanoparticles can easily be designed. Attractive laboratory experiments can be carried out with this apparatus, building a bridge between the fundamental statistical physics concepts introduced by Einstein in 1905 and novel applications in biophysics, bioengineering and, more generally, in nanoscience and nanotechnology.

ACKNOWLEDGMENTS

This work was funded by the Deutsche Forschungsgemeinschaft (SFB 569) and the University of Ulm. The correlator software will be made available to interested readers upon request.

APPENDIX: SELECTION OF COMPONENTS

The components were chosen to minimize the total cost of the apparatus without sacrificing too much in terms of performance. Excluding the computer, the essential components cost less than $6,000 (see Table I). The three essential parts of a fluorescence correlation spectroscopy setup are the laser, the microscope objective, and the detector.

We purchased a thermoelectrically cooled 20 mW DPSS 532 nm laser for ~$700. A poor quality laser beam shape can be tolerated because our built-in spatial filter ensures a high beam quality. We note that the power needed for the experiments is less than 1 mW. It may even be possible to use a green (or red) laser pointer as a light source, provided that its temporal stability suffices. Many low-cost lasers without optical feedback stabilization suffer from mode instabilities and power fluctuations, and therefore, one should carefully examine if the laser indeed provides the required stability.

The high-NA objective is normally one of the most expensive parts of a fluorescence correlation spectroscopy apparatus, with a price of several thousand dollars. We employed an oil immersion objective from Edmund Industrial Optics for about $300, which yielded surprisingly good results. Comparison with high-performance Zeiss and Olympus objectives showed that it could compete very well in this application.

Because of the single-molecule sensitivity of the technique, the photon counting detector is a crucial component. Photon counting modules based on silicon avalanche photodiodes feature quantum yields of up to 70% in the red spectral region, but their price of about $7000 would exceed the sum of all other components. We, therefore, chose a photon counting head (Hamamatsu H7155, ~$1850), which is based on a small metal package PMT. It is very compact, includes a high-voltage power supply, preamplifier, and discriminator and generates a TTL output pulse for each detected photon. Because of the large sensitive area of the PMT, there is no need for alignment of the detector. The detection yield of the PMT, however, is about five times smaller in the considered spectral range, which is still sufficient for fluorescence correlation spectroscopy experiments. Because the detector is the only component for which we sacrificed performance for cost reasons, its replacement by an silicon avalanche photodiode module is a straightforward modification, yielding a simple yet excellent fluorescence correlation spectroscopy instrument.

The metal and dichroic mirrors were purchased for only a few dollars, whereas we chose a high quality blocking filter to remove the scattered laser light as best as possible. Lenses, pinholes, and apertures are standard optical lab equipment. Many of the parts used for mounting were manufactured in the university's machine shop. Alternatively, the entire setup can easily be built using standard optical mounting material.

[1] A. Einstein, "Über die von der molekularkinetischen Theorie der Wärme geforderte Bewegung von in ruhenden Flüssigkeiten suspendierten Teilchen," Ann. Phys. **17**, 549–560 (1905).
[2] J. Perrin, *Les Atomes* (Félix Alcan, Paris, 1913).
[3] E. Haustein and P. Schwille, "Ultrasensitive investigations of biological systems by fluorescence correlation spectroscopy," Methods **29** (2), 153–166 (2003).
[4] D. Magde, E. L. Elson, and W. W. Webb, "Thermodynamic fluctuations in a reacting system – Measurement by fluorescence correlation spectroscopy," Phys. Rev. Lett. **29**, 705–708 (1972).
[5] R. Rigler, U. Mets, J. Widengren, and P. Kask, "Fluorescence correlation spectroscopy with high countrate and low background: analysis of translational diffusion," Eur. Biophys. J. **22**, 169–175 (1993).
[6] S. R. Aragon and R. Pecora, "Fluorescence correlation spectroscopy as a probe of molecular dynamics," J. Chem. Phys. **64**, 1791–1803 (1976).
[7] D. C. Lamb, A. Schenk, C. Röcker, C. Scalfi-Happ, and G. U. Nienhaus, "Sensitivity enhancement in fluorescence correlation spectroscopy of multiple species using time-gated detection," Biophys. J. **79** (2), 1129–1138 (2000).
[8] J. Wiedenmann, A. Schenk, C. Röcker, A. Girod, K. D. Spindler, and G. U. Nienhaus, "A far-red fluorescent protein with fast maturation and reduced oligomerization tendency from Entacmaea quadricolor (Anthozoa, Actinaria)," Proc. Natl. Acad. Sci. U.S.A. **99** (18), 11646–11651 (2002).
[9] L. Zemanova, A. Schenk, M. J. Valler, G. U. Nienhaus, and R. Heilker, "Confocal optics microscopy for biochemical and cellular high-throughput screening," Drug Discovery Today **8** (23), 1085–1093 (2003).
[10] L. Zemanova, A. Schenk, N. Hunt, G. U. Nienhaus, and R. Heilker, "Endothelin receptor in virus-like particles: ligand binding observed by fluorescence fluctuation spectroscopy," Biochemistry **43** (28), 9021–9028 (2004).
[11] A. Schenk, S. Ivanchenko, C. Röcker, J. Wiedenmann, and G. U. Nienhaus, "Photodynamics of red fluorescent proteins studied by fluorescence correlation spectroscopy," Biophys. J. **86** (1 Pt 1), 384–394 (2004).
[12] D. Magatti and F. Ferri, "Fast multi-tau real-time software correlator for dynamic light scattering," Appl. Opt. **40** (24), 4011–4021 (2001).
[13] D. Magatti and F. Ferri, "25 ns software correlator for photon and fluorescence correlation spectroscopy," Rev. Sci. Instrum. **74** (2), 1135–1144 (2003).
[14] Y. Chen, J. D. Müller, P. T. So, and E. Gratton, "The photon counting histogram in fluorescence fluctuation spectroscopy," Biophys. J. **77** (1), 553–567 (1999).
[15] P. Kask, K. Palo, D. Ullmann, and K. Gall, "Fluorescence-intensity distribution analysis and its application in biomolecular detection technology," Proc. Natl. Acad. Sci. U.S.A. **96** (24), 13756–13761 (1999).
[16] R. Reed, D. Holmes, J. Weyers, and A. Jones, *Practical Skills in Biomolecular Sciences* (Addison-Wesley Longman, Hong Kong, 1998).
[17] BSA was purchased from Sigma, St. Louis, MO.
[18] Oligonucleotides were custom ordered from MWG-Biotech (Ebersberg, Germany or Mendenhall, NC).
[19] R. P. Haugland, *The Handbook: A Guide to Fluorescent Probes and Labeling Technologies* (Molecular Probes, Eugene, OR, 2005), 10th ed. Streptavidin was purchased from Molecular Probes.